

## Quasi-Landau resonances in the spectra of rubidium Rydberg atoms in crossed electric and magnetic fields

G. Raithel, M. Fauth, and H. Walther

*Max-Planck-Institut für Quantenoptik and Sektion Physik der Universität München,  
D-8046 Garching, Federal Republic of Germany*

(Received 1 February 1991; revised manuscript received 5 April 1991)

This paper reports on the investigation of excitation spectra of rubidium Rydberg atoms in crossed electric and magnetic fields. The quasi-Landau spectra were evaluated and their Fourier transforms calculated. The scaled spectral scans used for this purpose were obtained by changing the electric and magnetic fields as well as the laser frequency in an appropriate way. The observed resonances could be explained completely by semiclassical orbits. Only orbits showing overlap with the ground-state wave function are observed. The polarization dependence of certain components in the Fourier spectra can be explained by the shape of the semiclassical orbits. The electric dipole moments of the atoms resulting from the shift of the quasi-Landau structures in a changing electric field agree quite well with the corresponding semiclassical orbits.

### I. INTRODUCTION

Recently spectra of Rydberg atoms in a strong external magnetic field and also in strong crossed electric and magnetic fields have attracted much interest, since the corresponding classical counterpart of such systems exhibits chaotic motion of the electrons.

Rydberg atoms in weak magnetic and weak crossed electric and magnetic fields were investigated theoretically by Solov'ev [1–3] and Braun [3,4] using perturbation theory. Based on this work Liberman, Pinard and co-workers explained the low-field spectra of lithium in weak magnetic fields and weak parallel electric and magnetic fields [5–10] Gay *et al.* [11,12] and Korevaar and Littman [13] investigated alkali-metal Rydberg atoms in weak crossed fields theoretically as well as experimentally.

If in higher magnetic fields the influence of the external field gets comparable to that of the inner-atomic field the atomic system gets classically chaotic. This is the regime which is of particular interest for the present work. In experiments with Rydberg atoms in that classically chaotic regime it was found that the excitation spectrum shows sinusoidal modulations of the spectral intensity. The most pronounced modulations in the so-called quasi-Landau (QL) region were first discovered by Garton and Tomkins in 1969 [14]. They occur near the ionization threshold in the  $P_z=1$  manifold ( $P_z$  represents the  $z$  parity) and exhibit a modulation in the spectra, the maxima of which are separated by about 1.5 times  $\hbar\omega_c$  ( $\omega_c$  is the cyclotron frequency). Above the ionization limit the separation approaches  $\hbar\omega_c$ . These resonances were explained by Edmonds and Starace using a semiclassical WKB approximation [15,16]. Later highly excited alkali-metal atoms were investigated in external magnetic fields using high-resolution laser techniques. Approaching the zero-field ionization limit strong lines appear being interpreted by Kleppner *et al.* as QL resonances

which were found to emerge from single quantum-mechanical states [17]. For higher excitation energies and higher external fields these resonances are broadened and appear as sinusoidal modulations the maxima of which follow WKB quantization in the plane perpendicular to the magnetic field [18,19]; they were in agreement with the original QL spectra of Garton and Tomkins and with the interpretation by Edmonds and Starace. It should be mentioned that there are also measurements performed on lithium Rydberg atoms in strong magnetic fields which exhibit QL resonances (for a review see Ref. [10]).

Broad resonances which can be understood semiclassically were also found in pure electric fields [20]. However, the Coulomb potential plus an external electric field is separable [21]. Therefore the reason for the smooth resonance structure at high energies is the short lifetime of the excited states. As shown in Ref. [20] the modulation maxima can be associated with single decay-broadened quantum-mechanical states. Rydberg atoms in external electric fields are not chaotic in the classical limit; this is a principle difference to the case of atoms in strong external magnetic fields. In the latter case the system is classically chaotic and it is important to state that in this case the modulation maxima resulting from the QL structure cannot be associated with single quantum states: the modulations are smooth envelopes over many energy levels which may be narrow and thus correspond to long-living states [22].

Further systematic experimental studies of QL spectra of hydrogen in strong magnetic fields were carried out by Welge and co-workers, and they identified in the Fourier transform of the spectra many new resonances besides the one showing a spacing between the successive modulation maxima of 1.5  $\hbar\omega_c$  [23–25]. It was possible to interpret these by semiclassical trajectories. In addition to the orbit which generates the QL resonances observed by Garton and Tomkins, and which spreads out in the plane

perpendicular to the magnetic field, other orbits extending in the same direction as the magnetic field were also observed.

The influence of classical trajectories on oscillator strength, level density, and wave functions was investigated theoretically by Gutzwiller [26–30], Berry [22], Reinhardt [31], Wintgen, Friedrich, and Hoenig [32–35], Wunner *et al.* [36], Heller [37], and Bogomolny [38]. A semiclassical theory developed by Du and Delos describing the average oscillator strength allows a quantitative comparison between experimentally obtained Fourier spectra and classical trajectory properties [39,40]. In crossed electric and magnetic fields an interesting class of electron trajectories spinning around the classical ionization saddle point was found [41] which will be discussed in connection with our results later.

The question arises whether the occurrence of the QL resonances is a general signature of the excitation spectra of Rydberg atoms in strong fields. Therefore, more detailed experiments are necessary, especially in cases where an additional electric field is applied perpendicular to the magnetic field. Crossed fields occur rather frequently, for example, in a plasma confined by a magnetic field or on the surface of neutron stars. Rydberg atoms are suited for laboratory experiments, since the experimentally achievable field strengths are comparable with the inner-atomic field acting on the Rydberg electron, therefore the strong-field regime can be achieved easily. Moreover, the high excitation energy of the Rydberg electron justifies semiclassical approximations of level density and wave functions. Such a simplified treatment is necessary, since up to now there have been no quantum-mechanical calculations available of spectra in strong crossed fields exceeding energies that correspond to those of levels with a principal quantum number of about 25.

## II. INFLUENCE OF CLASSICAL TRAJECTORIES ON QUANTUM PROPERTIES

### A. Modulations of the level density

Concerning the semiclassical description of the level density, we follow here the theory developed particularly by Gutzwiller [26–30]. He proceeds from a relation between the response function of a system and the respective propagator:

$$\begin{aligned} G(W) &= -i \int_{t=0}^{\infty} dt \int_V dx^n K(x, t, x, 0) e^{iWt} \\ &= \int_V dx^n \hat{G}(x, x, W), \end{aligned} \quad (1)$$

where  $K(x, t, x', 0)$  is the propagator,  $\hat{G}(x, x', W)$  the Green's function, and  $W$  the level energy. The response function  $G(W)$  on the left-hand side of Eq. (1) is defined by

$$G(W) \equiv \sum_a \frac{1}{W - W_a}. \quad (2)$$

The response function is closely related to the level density, which is essentially the imaginary part of  $G(W)$ . The summation in Eq. (2) is taken over all energy levels. The

integrand in the middle of Eq. (1) is the product of a phase factor and the propagator, starting at the position  $x$  and returning to  $x$  within a time  $t$ . The propagator is written as a Feynman path integral. By successively employing the stationary phase approximation Gutzwiller ends up in a semiclassical expression  $G_{\text{SC}}(W)$  for  $G(W)$  which essentially contains a sum over all classical periodic orbits (PO). His result for two-dimensional systems is written [29]

$$G_{\text{SC}}(W) = \sum_{\text{PO}} \frac{-iT}{2\hbar} \sum_{m=1}^{\infty} \frac{1}{2 \sinh(m\beta/2)} e^{im[S(W)/\hbar - n\pi/2]}; \quad (3)$$

$T$  stands for the revolution time along the periodic orbits and the summation index  $m$  corresponds to the number of revolutions along one periodic orbit. The parameter  $\beta$  depends on the stability of the orbits PO:  $\beta$  is purely imaginary for stable orbits, and is real and greater than 0 for unstable orbits. The parameter  $S$  denotes the energy-dependent action integral over one traversal, and  $n$  is the number of conjugate points along the orbit in the case of unstable orbits; for stable orbits  $n$  is zero. For the three-dimensional case the coefficients of the phase terms in Eq. (3) are getting more complicated, since the description of the stability of the trajectories requires more parameters than just  $\beta$ .

From the relation  $dS = T dW$  which is well known from classical mechanics follows that periodic orbits cause modulations of the level density whose periods on the frequency scale are equal to the revolution frequencies. Unstable orbits generate sinusoidal modulations, since the coefficients of the phase terms in Eq. (3) decrease rapidly with increasing number of revolutions; this is not the case for stable orbits where the coefficients do not decrease. Therefore, stable orbits lead to a level density corresponding to periodic linelike structures. In this limit the more general Gutzwiller treatment approaches the semiclassical treatment of Bohr and Sommerfeld being only applicable to integrable systems [29]. Thus the structure of the mean level density is related to the classical stability behavior of the system.

It must be pointed out that the stationary phase approximation which is applied here requires that the system can be semiclassically approximated anywhere in its configuration space. The introduction of a scattering center such as the Coulomb potential which cannot be described in semiclassical terms leads to the requirement to use the quantum-mechanical expression of the Green's function in its vicinity. Therefore the momentum of an electron which closely approaches the scattering center is changed abruptly in any direction, whereby the probability for a particular momentum transfer follows the laws of quantum mechanics. Therefore the scattering center leads to the occurrence of trajectories in Gutzwiller's formula Eq. (3) which are classically not periodic. The amplitudes of the level density modulations caused by those trajectories depend not only on their classical stability behavior, but also on the quantum-mechanical differential scattering cross section at the scattering center.

### B. Modulations of the excitation cross section

In an experiment where the QL structure is examined, the intensity modulation of the excitation spectra, not the level density, is investigated. Therefore the dipole matrix elements connecting ground and Rydberg states determines the results. A formalism which approximates the mean excitation cross section semiclassically was developed by Lu and Delos [32,40]. They calculated the mean excitation cross section of hydrogen in a strong magnetic field starting with a well-known relation between oscillator strength and the Green's function:

$$f(W) = -\frac{2m_e(W - W_i)}{\pi\hbar^2} \text{Im} \langle D\psi_i | G_W^\dagger | D\psi_i \rangle$$

with

$$D = \mathbf{D} \cdot \mathbf{e}_{\text{pol}}. \quad (4)$$

$W$  and  $W_i$  denote the energies of the excited state and the ground state  $|\psi_i\rangle$ , respectively.  $D$  is the projection of the dipole operator  $\mathbf{D}$  onto the direction of the laser polarization. The Green's function  $G_W^\dagger(\mathbf{q}_f, \mathbf{q}_i)$  has a semiclassical approximation [39,40]:

$$G_W^\dagger(\mathbf{q}_f, \mathbf{q}_i) = c \sum_{\text{cl}} |\rho_{\text{cl}}(\mathbf{q}_i, \mathbf{q}_f)|^{1/2} \times \exp \left[ \frac{iS_{\text{cl}}(\mathbf{q}_i, \mathbf{q}_f)}{\hbar} - i\frac{n_{\text{cl}}\pi}{2} \right], \quad (5)$$

where the sum is taken over all classical trajectories connecting the initial point  $\mathbf{q}_i$  and the final point  $\mathbf{q}_f$ . The classical functions  $S_{\text{cl}}(\mathbf{q}_i, \mathbf{q}_f)$  and  $\rho_{\text{cl}}(\mathbf{q}_i, \mathbf{q}_f)$  denote the action integrals along the trajectories and the modulation amplitudes depending on the classical stability of the trajectories. Lu and Delos evaluate Eq. (4) applying the quantum-mechanical Coulomb Green's function (without external fields) within a tiny sphere surrounding the proton, and the semiclassical Green's function Eq. (5) outside the sphere, but now including the external field. Their result approximating the energy averaged oscillator strength in the vicinity of the field-free ionization limit is [29,40]

$$f(W) = f_0(W) + \sum_{\text{cl}} C_{\text{cl}} \sin(T_{\text{cl}}W + \Delta_{\text{cl}}), \quad (6)$$

where  $f_0(W)$  is the field-free energy-averaged oscillator

strength. The sum is taken over all recurring trajectories.  $T_{\text{cl}}$  are the times of traversal and  $\Delta_{\text{cl}}$  are trajectory dependent phases. In Refs. [39] and [40] the modulation amplitudes  $C_{\text{cl}}$  are calculated which depend on the stability behavior of the orbits, the ground-state quantum numbers, and the laser polarization. In contrary to Eq. (3) Eq. (6) contains not only periodic orbits which can be traversed many times but also recurring orbits which can be traversed only once by a classical electron. There is no difference in the calculation procedure of the amplitudes  $C_{\text{cl}}$  which favors the periodic orbits with respect to trajectories which are only recurring [39,40]. The derivation of the Gutzwiller formula Eq. (3) however suggests that also in a semiclassical expression of the oscillator strength applied to systems fulfilling semiclassical conditions anywhere in configuration space the recurring trajectories can be ruled out by a stationary phase argument. Therefore the influence of recurring trajectories should vanish if the nonclassical Coulomb center would disappear.

Since the atoms which are examined in our experiments always contain the Coulomb center the purely semiclassical case treated by Gutzwiller is not realized there. Therefore we expect that recurring as well as periodic orbits modulate the excitation spectra. Nevertheless, our experiments show that the spectra are dominated by periodic orbits, especially for high action values, i.e., short-range modulations. The reason for that may be that the classical amplitudes  $C_{\text{cl}}$  tend to get large if a trajectory is periodic or nearly periodic.

### C. Semiclassical probability distributions

The connection between excitation cross section and semiclassical orbits which could be traversed by an excited classical electron suggests that also the wave functions of excited states in the Rydberg regime which are expected to exhibit some classical behavior, are affected by semiclassical trajectories. Bogomolny found by working out the semiclassical approximation of Green's function Eq. (5) that such a correlation between wave functions and periodic orbits exists [38]: the slightly space and energy averaged quantum-mechanical probability distributions can be semiclassically approximated by a mean part plus contributions resulting from periodic orbits:

$$\langle |\psi(q)|^2 \rangle = \rho_0(q) + \hbar^{n-1/2} \sum_{\text{PO}} \text{Im} \left\langle A_{\text{PO}}(x) \exp \left[ \frac{i}{\hbar} \left( S_{\text{PO}} + W_{\text{PO}}^{km}(x) \frac{y_k y_m}{2} \right) \right] \right\rangle. \quad (7)$$

Here  $n$  is the dimensionality of the system, and  $x$  and  $y_i$  designate space coordinates in a system where the  $x$  axis is taken along the periodic orbits and the  $y_i$  in transversal direction. The mean part  $\rho_0(q)$  is the projection of the classical microcanonical distribution onto the configuration space, whereas the probability distribution is enhanced in the neighborhood of periodic orbits. The strength of these enhancements depends on the stability of the orbits via  $A_{\text{PO}}(x)$  and  $W_{\text{PO}}^{km}(x)$  in Eq. (7) which are functions of the monodromy matrix of the periodic or-

bits. Equation (7) was derived for systems exhibiting unstable periodic orbits and fulfilling semiclassical conditions anywhere in configuration space. The introduction of a Coulomb center would lead to the appearance of recurring orbitals in Eq. (7) (see II A). Since in the experiment transitions from the ground state localized at the Coulomb center to large Rydberg states are measured, the measurement is sensitive only to wave-function enhancements generated by trajectories performing at least one close approach to the core. Therefore also the

semiclassical approximation of wave functions suggests that classical periodic and recurring orbits which approach the Coulomb center show up as periodic modulations in the excitation spectrum.

### III. EXPERIMENTAL EXPLANATION OF QUASI-LANDAU SPECTRA

The aim of our experiment was to investigate the QL spectrum of rubidium Rydberg atoms and to identify the corresponding semiclassical orbits. If the excitation spectra are recorded using fixed field values, the Fourier transforms of the spectra yield the revolution times of the corresponding semiclassical trajectories. This follows from the relation  $dS = T dW$  and Eq. (6). However, the useful energy range over which the Fourier transform can be taken is limited for two reasons.

- (1) The revolution times of the semiclassical trajectories change with the excitation energy.
- (2) In most cases the amplitudes  $C_{cl}$  in Eq. (6) change quite rapidly as a function of the energy. Therefore generally the modulations due to one type of trajectories appear only in a small energy range, thus no accurate value of the revolution times can be deduced.

For those reasons ordinary spectra allow us only in some cases to identify the trajectories which modulate the spectra.

In order to circumvent this difficulty it is necessary to employ a classical scaling property of the examined system, which is discussed in the following. The real parameters determining the motion of the electron are the energy  $W$  and the field values  $E$  and  $B$ . The Hamiltonian of the system in terms of these parameters is

$$H = \frac{p^2}{2} - \frac{1}{r} - Ex + \frac{B}{2}l_z + \frac{B^2}{8}(x^2 + y^2), \quad (8)$$

with  $\mathbf{E} = -E\mathbf{e}_x$  and  $\mathbf{B} = B\mathbf{e}_z$ .

Transforming to scaled coordinates, energy and electric field according to

$$\begin{aligned} \varepsilon &= EB^{-4/3}, \quad \omega = WB^{-2/3}, \\ \mathbf{r}_s &= \mathbf{r}B^{2/3}, \quad \mathbf{p}_s = \mathbf{p}B^{-1/3} \end{aligned} \quad (9)$$

leads to the scaled Hamiltonian  $H_s$

$$H_s = \frac{p_s^2}{2} - \frac{1}{r_s} - \varepsilon x_s + \frac{1}{2}l_{z,s} + \frac{1}{8}(x_s^2 + y_s^2), \quad (10)$$

which does not depend on  $B$ . One trajectory solving Eq. (10) corresponds to a one-dimensional manifold of trajectories solving Eq. (8).

A so-called scaled spectrum is taken at constant scaled energy and scaled electric field. The scaled spectrum is recorded in a fixed energy range  $[W_0, W_1]$ . The real field values which have to be applied to the atoms during the scan change in order to provide constant scaled parameters  $\varepsilon$  and  $\omega$  [see Eq. (9)]. As mentioned above only those trajectories result in a modulation of the spectra which approach the core region. During the scan the trajectories following from Eq. (10) are kept unchanged,

whereas the corresponding trajectories solving Eq. (8) evolve according to the scaling laws, that means they keep their shape, but they are reduced or blown up depending upon whether the energy  $W$  is increased or decreased.

The scaled action  $S_s$  of a trajectory is given by  $S_s = SB^{1/3}$ ; this follows from  $S = \int \mathbf{p} \cdot d\mathbf{q}$  and Eq. (9). Therefore the action  $S$  of the trajectory changes proportionally to  $B^{-1/3}$  during the scaled scan. Since  $S$  changes by  $h$  between successive modulation maxima, they exactly appear equidistant on a  $B^{-1/3}$  scale. This is the main advantage of scaled spectra. The modification of Eq. (6) for scaled spectra recorded as a function of  $B^{-1/3}$  yields

$$f(B^{-1/3}) = f_0(B^{-1/3}) + B^{1/6} \sum_{cl} C_{s,cl} \sin(B^{-1/3} S_{s,cl}). \quad (11)$$

$C_{s,cl}$  are complex scaled modulation amplitudes, containing also the Maslov index. The  $C_{s,cl}$  keep constant during the whole scaled scan as well as the scaled action values  $S_{s,cl}$  of the trajectories. The only dependence of the modulation strength on  $B$  is via  $B^{1/6}$  which is proportional to  $W^{1/4}$ . Since this is a very weak dependence a trajectory influencing the scaled spectrum at its beginning does so within the whole energy range  $[W_0, W_1]$  of the scaled scan. Therefore the Fourier transforms of long-scaled spectra yield values of the actions of the modulating trajectories being accurate enough so that they can be identified.

### IV. EXPERIMENT

The experimental setup is shown in Fig. 1. Our experiments have been performed with rubidium Rydberg atoms; these are much simpler to investigate than hydro-

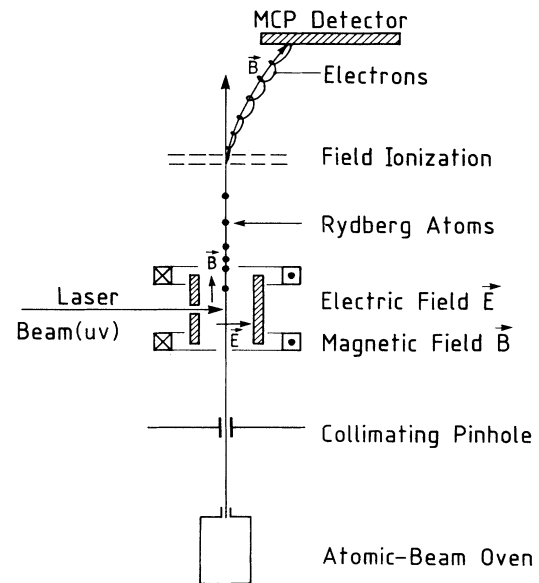


FIG. 1. Experimental setup.

gen atoms, and furthermore the spectra can be recorded with a much higher resolution. The use of rubidium atoms is no disadvantage since they also represent a one-electron system for which the pure Coulomb field is only disturbed when the valence electron is inside the core. This disturbance however has no influence on the QL spectra, as has been shown by O'Mahony for Li and Sr atoms in strong magnetic fields [42].

The excitation of the rubidium Rydberg levels was performed by the frequency doubled radiation of a dye laser (rhodamine 6G). The rubidium atoms emerge from an atomic beam oven and pass through strongly collimating pinholes. In the excitation region well-defined electric and magnetic fields are present. In order to avoid a motional electric field ( $\mathbf{v} \times \mathbf{B}$  contribution) the atomic beam is directed parallel to the magnetic field which is generated by a superconducting pair of coils. The laser beam crosses the atomic beam at right angles. The residual Doppler width amounts to 15 MHz. About 200  $\mu\text{s}$  after the excitation all Rydberg atoms are field ionized, and the stray magnetic field deflects the field electrons onto a microchannel plate detector. With this experimental setup the excitation rate of Rydberg atoms is recorded. The laser frequency and the field values are varied by a computer which is also used to add the signal counts into a set of channels. The Fourier transforms of the spectra yield the revolution times of the semiclassical orbits or, in the case of scaled spectra, the values of the action of the modulating trajectories.

### V. EXCITATION SPECTRA AT A MAGNETIC FIELD OF 0.7 T

In order to get a survey on the spectra at 0.7 T recordings were made covering an energy range from principal

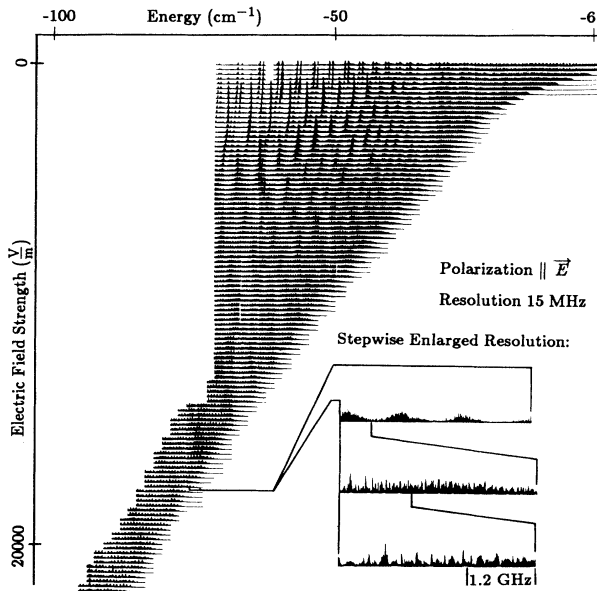


FIG. 2. Rubidium spectrum for  $B=0.7$  T in the energy range  $-103$ – $-5$   $\text{cm}^{-1}$ . The recording displayed in one line was taken at a constant electric field. The electric field increases from line to line by 200 V/m.

quantum numbers 33 to about 150. The laser polarization was parallel to the electric field, which was increased progressively in steps of 200 V/m starting at zero value and ending at the ionization field strength. The spectrum shown in Fig. 2 was assembled by putting many sections together. Therefore, the spectrum shown in Fig. 2 is highly reduced in size and therefore only the coarse features can be recognized. The insert demonstrates the actual resolution on an extended scale (linewidth 15 MHz).

The spectra show structures which are composed of sharp and nearly equidistant lines in the region where the external fields have smaller influence (upper left corner of the recording Fig. 2; this corresponds to the situation investigated, e.g., in Ref. [17]). However, in the regions with strong influence of the external fields the QL structures appear as sinusoidal envelopes of a very dense spectrum. According to the formula of Gutzwiller [Eq. (3)] this change of the QL structure between the two types (linelike structures and sinusoidal modulations) reflects the transition of the dynamics of the corresponding classical system from regular to chaotic. Thus the structure of the QL spectrum provides also information on the classical analog.

At first glance, two long-periodic sets of QL structures with a period of about three to five times the cyclotron frequency can be recognized in Fig. 2 or more clearly in Fig. 3 where sections of Fig. 2 are shown. The two sets differ in the apparent dipole moment, according to which the QL structures shift when the electric field is changed. This means Fig. 2 exhibits the Stark map of the QL resonances. The behavior of the coarse QL structure is explained by the trajectories shown in Fig. 3; they determine mainly the QL structure in the spectral region displayed in Fig. 3.

When the electric field is reduced to zero value both orbits change into the trajectory originally observed by Garton and Tomkins. In order to prove that these orbits explain the coarse QL structure, the action was calculated as a function of energy and electric field. It differs by  $h$  for the different neighboring straight lines superposed to the spectra of Fig. 3; the positions of the maxima of the coarse QL structures coincide with these lines. Furthermore, the slopes of these lines are consistent with the dipole moments corresponding to the respective trajectories. This is proof also that these trajectories generate the coarse QL structure, as can be understood from Ref. [40], Appendix C, yielding in our case, where the Hamiltonian contains an electric-field term  $-eEx$ :

$$\frac{\partial S}{\partial E} = dT$$

with trajectory dipole moment  $d$ . The application of  $(\partial x / \partial y)|_f = -(\partial f / \partial y)|_x / (\partial f / \partial x)|_y$ , valid for any  $f(x, y)$  yields

$$\frac{\partial W}{\partial E} = -d.$$

Our data and the orbits displayed in Fig. 3 fulfill this relation.

It must be pointed out that the trajectories shown in

Fig. 3 return to the core, but they are not periodic as most of the other trajectories which modulate the spectrum and which are shown below. The discussion of the role of periodic and recurring orbits in II suggests that systems which can be semiclassically approximated anywhere in configuration space are influenced only by periodic orbits, whereas violations of the semiclassical conditions lead to the occurrence of modulations generated by trajectories which are only recurring. Therefore the orbits shown in Fig. 3 are able to modulate the spectrum due to the nonclassical scattering of the returning electron at the Coulomb center.

The spectrum exhibits also modulations of finer structure with a period of about 0.5 to 1 times the cyclotron frequency (see insert of Fig. 2). The trajectories generating these modulations could be identified only by means of scaled spectra which will be discussed in the following.

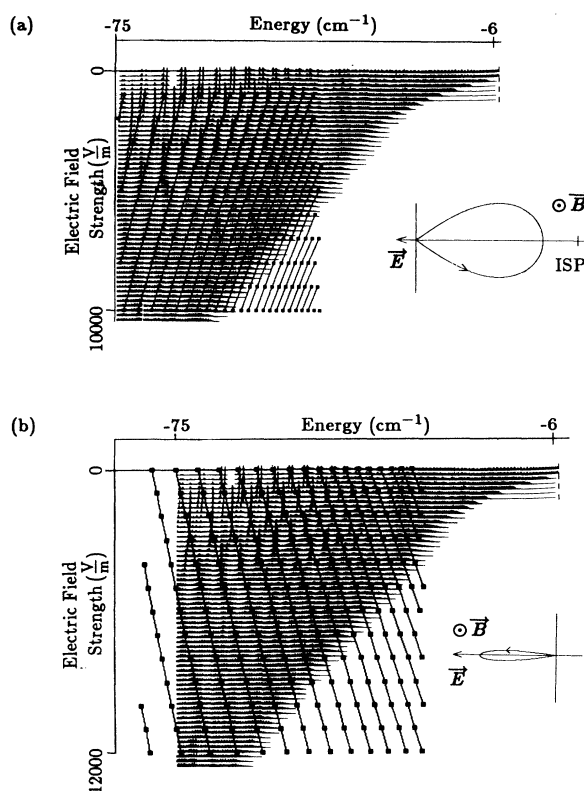


FIG. 3. Coarse QL structure of the spectra at  $B=0.7$  T (see also Fig. 2). The modulation maxima are connected by solid lines. The meaning of these lines is explained in the text. In (a) the lines connect modulation maxima that are generated by the orbit which is oriented in the opposite direction of the electric field. The trajectory is shown in the right-hand side. The dipole moment of the lines and of the trajectory is about  $1400 e \text{ \AA}$ . In order to visualize the size of the trajectory the position of the classical ionization saddle point (ISP) is indicated. In (b) the second type of coarse modulations are enhanced by solid lines. They are generated by a trajectory which is lying in the direction of the electric field. The modulations and the corresponding trajectory show a dipole moment of about  $-1000 e \text{ \AA}$ .

## VI. SCALED SPECTRA, FOURIER ANALYSIS, AND TRAJECTORIES

The introduction of the scaling procedure allow us to reduce the number of parameters describing the spectra from three to two. In addition, the measurements were restricted to the region close to the ionization threshold, that means for the scaled energy [Eq. (9)] we chose the maximum possible value. Therefore only one important parameter remains, the scaled electric field, corresponding essentially to the influence of the electric field in comparison with that of the magnetic field. Two limiting cases will be discussed here: dominating electric field and dominating magnetic field.

First the case of large electric field is discussed. In order to give an impression of the scaled spectra before Fourier transformation Fig. 4 shows a series of them taken for the scaled parameters and energy range as indicated. In order to visualize the influence of the different terms in the Hamiltonian their magnitudes are shown in Fig. 4 for a region far away from the core. These values show that the external fields and the inter-atomic field are of comparable size. The spectrum at the upper left of Fig. 4 was taken for parameters for which only a few excited Rydberg states are stable enough to be detected. It must be pointed out that due to the scaling procedure this situation keeps the same for the entire scaled spectrum. The following spectra of Fig. 4 are taken at the same scaled electric field and for successively increasing

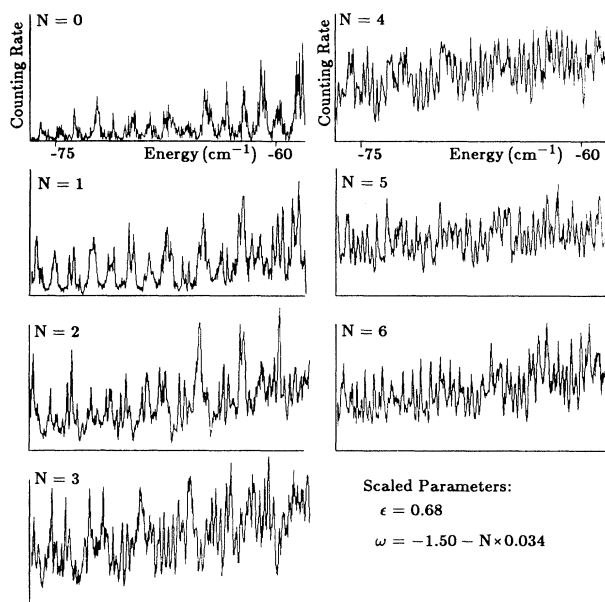


FIG. 4. Scaled spectra with initial parameters  $E=8196$  V/m,  $B=0.45$  T,  $W=-50.8 \text{ cm}^{-1}-N \times 0.55 \text{ cm}^{-1}$ , where  $N$  designates the numbering of the spectra starting on the left-hand side from above. The laser polarization is parallel to the electric field. Far away from the core the orders of magnitude of the different terms in the Hamiltonian are (in a.u.) as follows: Coulomb term,  $2 \times 10^{-4}$ ; electric field,  $8 \times 10^{-5}$ ; diamagnetic term,  $1 \times 10^{-5}$ .

scaled energy  $\omega$ , being equivalent to increasing stability of the atoms with respect to field ionization. The following coarse features can be recognized. (1) Close to the ionization threshold (spectra at the upper left of Fig. 4) components at small values of  $S_s$  dominate (i.e., with long wavelengths). (2) With decreasing scaled energy (lower right of Fig. 4) one component with a short wavelength and one with a very long wavelength are dominating.

Therefore it can be stated that the different QL resonances exhibit different stability behavior or, in other words, the stability of the wave functions is differently affected by the corresponding semiclassical trajectories making the excited states more or less sensitive to decay into the continuum. A possible explanation of this feature is that the different influences lead to a different amplitude of the oscillatory wave function beyond the ionization saddle point and therefore to different ionization probabilities.

The Fourier transforms of the scaled spectra reveal the detailed QL structure of the scaled spectra. Figure 5 shows the Fourier spectra obtained from the spectra in Fig. 4. In the diagram the resonance strength is plotted versus the scaled action which is displayed in units of  $h$ . Figure 5 demonstrates clearly that the scaled spectra in Fig. 4 can be decomposed into a set of well-separated sharp resonances. As will become clear later it is useful to collect the resonances in groups which correspond to different types of generating trajectories. This is included in Fig. 5.

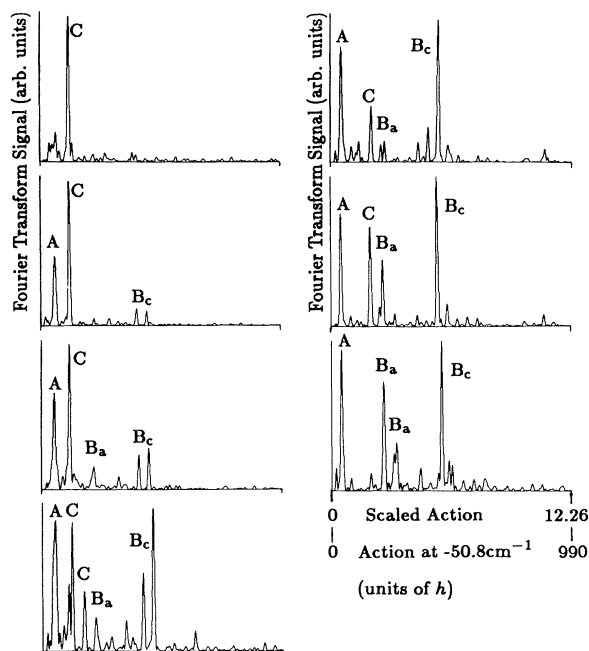


FIG. 5. Fourier spectra of the scaled spectra shown in Fig. 4. In the diagrams the square of the Fourier amplitude is plotted the scaled action and the action of the modulating trajectories at an energy of  $-50.8 \text{ cm}^{-1}$ . Individual resonances or groups of resonances are labeled by letters which are referred to in the text.

If the polarization is changed, a new group of resonances shows up in the gap between the resonances labeled by  $B_a$  and  $B_c$  in Fig. 5. In addition, the resonances  $B_a$  and  $B_c$  themselves almost disappear (see Fig. 6).

In the following sections the trajectories generating the modulations displayed in Figs. 5 and 6 will be discussed. The resonance at  $50h$  appears for each polarization and is caused by the trajectories which are already shown in Fig. 3.

For each polarization two strong resonances appear (labeled by C) over a rather large range of parameters at scaled actions of  $1.52h$  and  $2.14h$ . They are generated by trajectories which approach the core once per revolution and which are periodic in phase space. Figure 7 shows the shapes of some orbits belonging to that group. Due to the symmetry of the system, the orbits approach the core in the direction of the electric field. Figure 7 also indicates the scaled electric field at which these orbits occur, and the scaled energy, at which the orbits closely approach the core. Changing the scaled energy at which an individual orbit approaches the core causes a deformation of this orbit leading to an increased distance between orbit and core. As well as for other orbits experimentally a relation between the resonance strengths and the core distance of the associated orbits was found. The smaller the spacing between the associated orbit and the core the stronger the resonances. Figure 7 shows that only the trajectories  $C_1$  and  $C_2$  approach the core within the experimentally examined parameter range. Therefore this explains why only the orbits  $C_1$  and  $C_2$  were found to

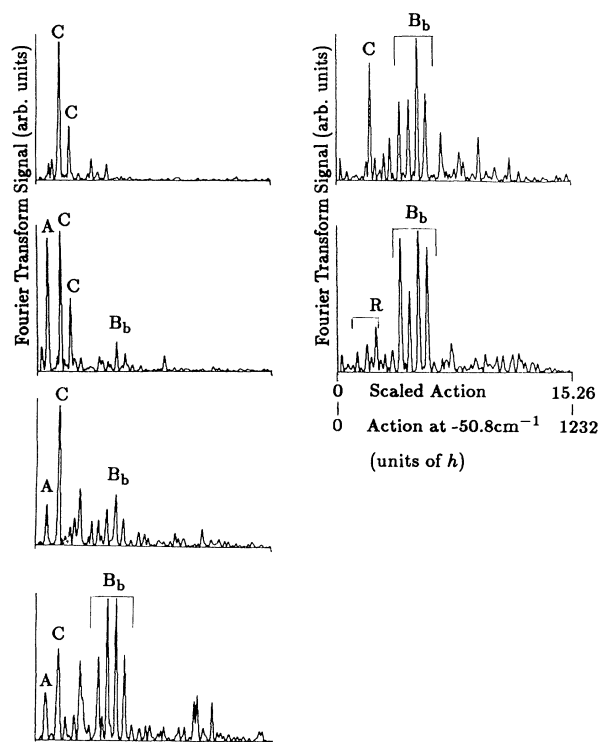


FIG. 6. Fourier spectra with the same parameters as in Fig. 5 (without  $N=6$ ), but polarization perpendicular to  $E$  and  $B$ .

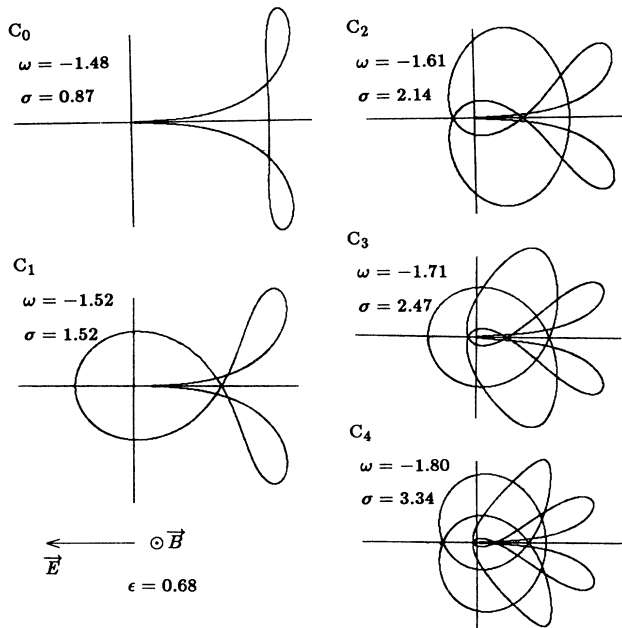


FIG. 7. Modulating periodic trajectories which approach the core once per revolution (not complete). The scaled parameters and the values of scaled action  $\sigma$  of the trajectories in units of  $h$  are indicated. Only the trajectories  $C_1$  and  $C_2$  are in the experimentally covered range.

generate modulations in the observed spectra. The trajectories shown in Fig. 7 besides  $C_1$  and  $C_2$  would generate modulations at the corresponding scaled energies indicated there.

There exists an interesting group of trajectories which

can be derived from orbit  $C_0$  shown in Fig. 7. They are closely related to the so-called quasi-Penning orbits (QP orbits) described by Clark, Korevaar, and Littman [41]. These unstable closed loops around the classical ionization saddle point exhibit an amazing feature; they extend far into the region beyond the classical ionization saddle point. They were supposed to modulate the photoabsorption cross section in crossed magnetic and electric fields [41]. However, according to Sec. II B, trajectories modulating the excitation spectrum have to start at the core region and return to it. Therefore, the genuine QP orbit may modulate the level density, but not the excitation spectra starting from low-lying initial states (this is the experimental situation encountered in high-resolution laser spectroscopy). Nevertheless, it is possible to approach the QP orbits by recurring trajectories. Slight changes of the initial parameters of trajectory  $C_0$  (Fig. 7) lead to trajectories performing an arbitrary number of loops around the ionization saddle point (Fig. 8). However, the energy above which these orbits exist is a couple of wave numbers above the ionization limit; therefore the spectra presented in this paper exhibit no signature of them. They have another disadvantage: their stability decreases strongly as the number of loops increases. A calculation of modulation amplitudes according to Refs. [39] and [40] yields that only the first few trajectories shown in Fig. 8 should be stable enough to result in detectable modulations. Scaled spectra above the ionization limit that might be modulated by these orbits are planned to be the subject of future work.

Nearly all the other resonances which occur in the right part of the Fourier spectra of Figs. 5 and 6 are generated by trajectories approaching the core twice per revolution (Fig. 9). For the same reason that applies to the C-type trajectories there exist more trajectories of this

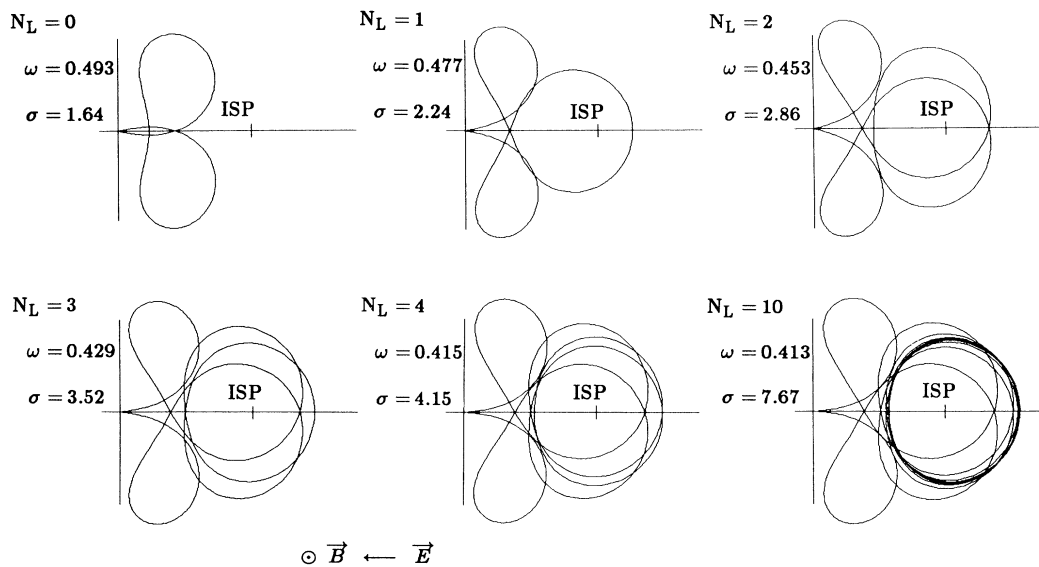


FIG. 8. Trajectories which approach the Quasi-Penning orbit calculated with a scaled electric field of  $\epsilon=0.235$ . They are labeled by the number of loops  $N_L$  around the classical ISP, the scaled energy, and the scaled action. The first few trajectories shown may result in a modulation of the absorption spectrum above the ionization limit.

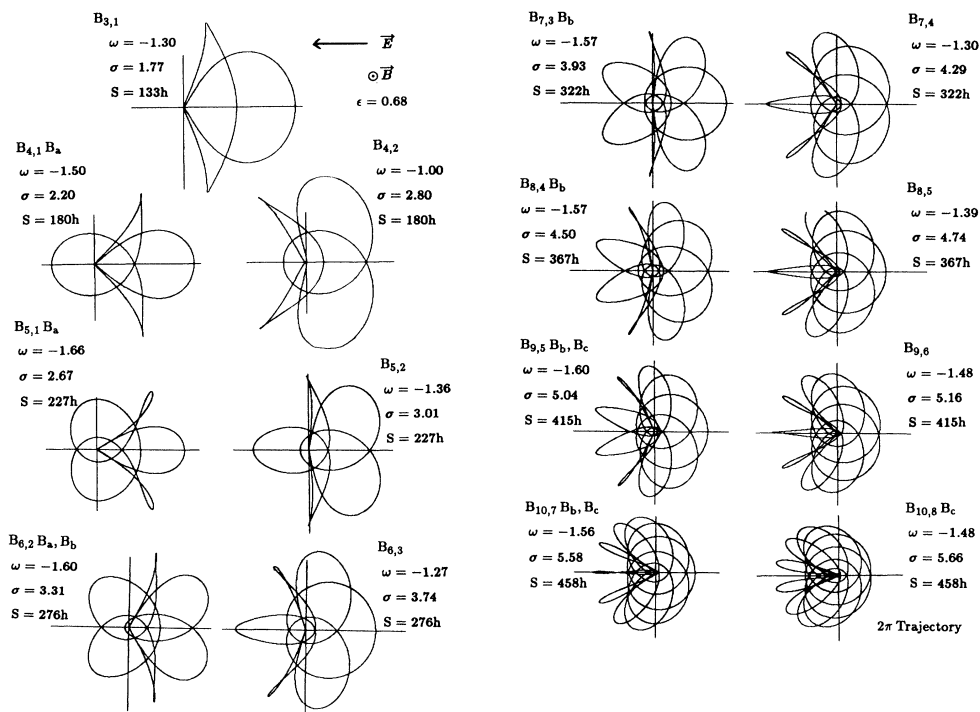


FIG. 9. Modulating periodic trajectories approaching the core twice per revolution (uncomplete). The scaled parameters and the values of scaled action  $\sigma$  of the trajectories are indicated. Additionally the values of the action at an energy of  $-50.8 \text{ cm}^{-1}$  are shown. The trajectories are labeled by a descriptor showing the total number of loops of the trajectories (first number in subscript) and the number of loops which lie in the right part of the trajectories between the two points of closest approach to the core (second number in subscript). For trajectories which influence the spectra in the experimentally covered parameter range also the corresponding resonance type ( $B_a - B_c$ ) is shown.

type than observed in the experiment. Furthermore, for most trajectories approaching the core twice there are a couple of orbits having the same action calculated for a fixed energy. A few of them are shown in Fig. 9. The orbits which are believed to generate a modulation are additionally labeled by the group of resonances they can be associated to.

In most Fourier spectra of Fig. 5 one resonance of type  $B_c$  strongly dominates. It corresponds to the orbit  $B_{10}$  ( $2\pi$  trajectory) in Fig. 9, where the electron starts more or less in direction of the electric field, traverses many lobes the orientation of which perform a full  $2\pi$  circle, and finally returns to the core running counter to the electric-field direction. For other parameters than those of Fig. 5 the orbit starting in the electric-field direction may consist of more or less than 10 lobes, but further experimental results show that over a wide parameter range it has an outstanding resonance strength. Thus the fine modulations which are mentioned at the end of Sec. V are generated by the  $B$ -type orbit starting in the electric-field direction.

As already mentioned the strengths of resonances belonging to the groups  $B_a - B_c$  depend on the laser polarization. Figure 10 illustrates that influence for three individual resonances which are typical examples of the groups  $B_a - B_c$ . The upper orbit in Fig. 10 is favored when the polarization is perpendicular to the electric field, and the other two when it is parallel. Generally the

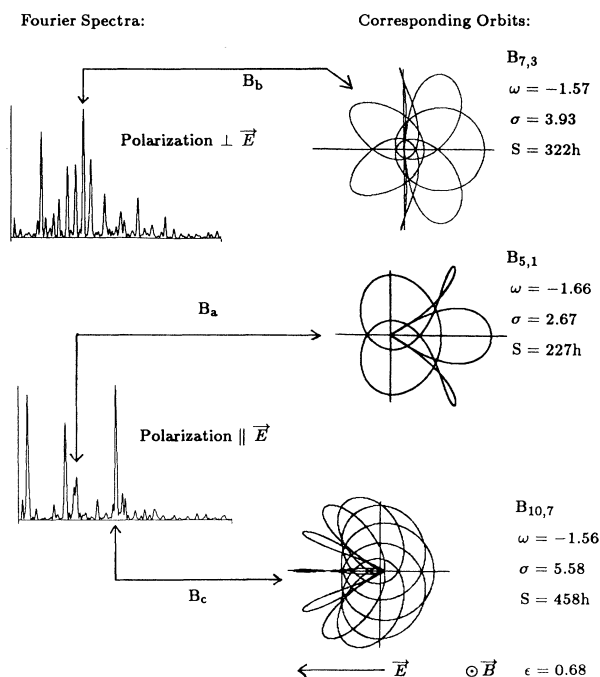


FIG. 10. Polarization dependence of the resonance strength. The resonance strength is the stronger the smaller the angle between laser polarization and the part of the trajectories along which the electron approaches the core is.

angle  $\alpha$  between laser polarization and the part of the orbit along which the electron approaches the core is smaller the stronger the associated resonance is. The interpretation of this feature is straightforward: the light polarization determines the direction in which the excited wave function is enhanced. The coefficients  $C_{cl}$  in Eq. (6) also include terms which depend on the laser polarization and ground-state quantum numbers. In our case the ground state is the  $5s$  state which leads to an angular dependence of the squares of the Fourier amplitudes proportional to  $\cos^4(\alpha)$ , where  $\alpha$  is the angle defined above. This coincides with our observations.

The Fourier spectra show that there are parameter regions where only one or two resonances dominate. In such a region the QL structure of the ordinary spectrum is quite simple and regular. Therefore, the variation of the QL structure can easily be seen when the external electric field is changed. Figure 11 shows a typical example: on the right of the displayed ordinary spectrum the  $C_1$  resonance shows up whereas on the left the resonances caused by the  $B_{10}$  orbit (see Fig. 9) can be seen. It is possible to calculate the spectroscopic dipole moments resulting from the Stark structure of the QL modulations. The dipole moments obtained by the spectrum agree with that of the trajectories assigned to the resonances. This is

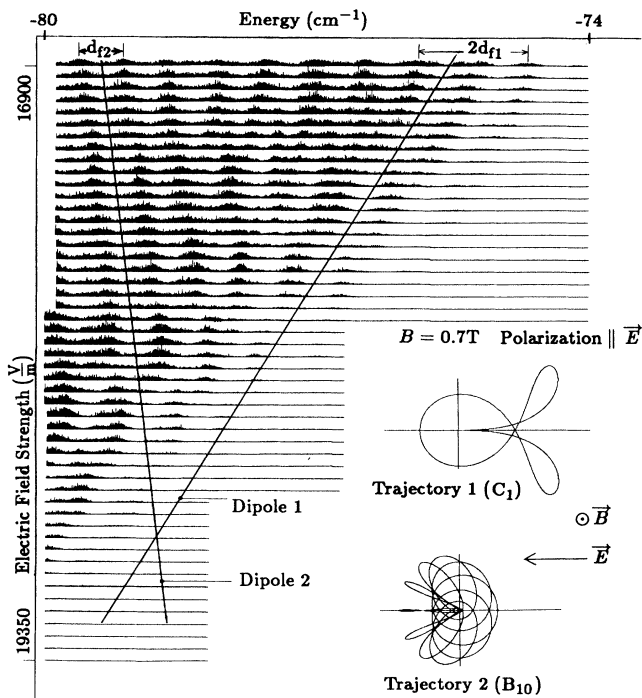


FIG. 11. Comparison between spectroscopic dipole moments of the modulations and dipole moments of the corresponding trajectories. The magnetic field was  $B=0.7$  T. Specific values for trajectories 1 and 2, respectively, are as follows: Spectroscopic dipole moment,  $1700 \pm 200$  A and  $-450 \pm 70$  A; trajectory dipole moment,  $1500 \pm 100$  A and  $-400 \pm 50$  A;  $1/d_f$ ,  $(1.0 \pm 0.1)T_c$  and  $(1.4 \pm 0.1)T_c$ ; revolution time,  $(1.05 \pm 0.07)T_c$  and  $(1.22 \pm 0.07)T_c$ .

another proof that the calculated trajectories explain the observed QL resonances.

In the preceding sections we discussed spectra with quite high scaled electric field. In the following we will discuss the case of strongly dominating magnetic field, i.e., low scaled electric field. In these cases the Fourier transforms of the scaled spectra consist of an equidistant set of resonances, as shown in Fig. 12. The Fourier spectra shown there are arranged in the same manner as those in Figs. 5 and 6. The observed resonances correspond to values of the action which are integral multiples of that of the quasi-Landau-orbit observed by Garton and Tomkins, since the influence of the magnetic field dominates and the electric field can be considered as a small perturbation. This can be seen in Fig. 13 where some high magnetic field orbits are plotted which are extending in the plane perpendicular to the magnetic field. The shape of their loops only slightly deviates from the quasi-Landau-orbit originally observed by Garton and Tomkins.

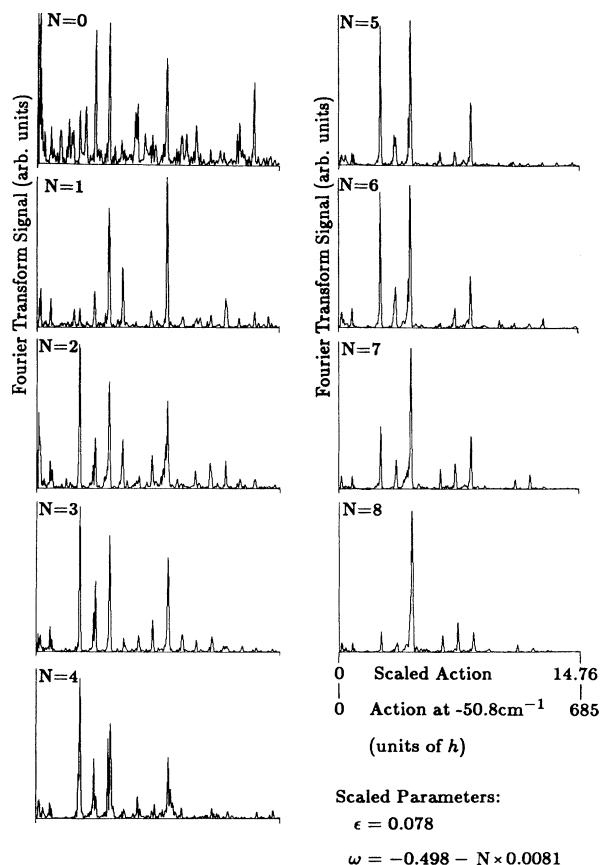


FIG. 12. Fourier spectra of scaled spectra with initial parameters  $E=8718$  V/m,  $B=2.36$  T,  $W=-50.8$   $\text{cm}^{-1} - N \times 0.83$   $\text{cm}^{-1}$ , where  $N$  designates the numbering of the spectra starting on the left side from above. The laser polarization is parallel to the electric field. Far away from the core, the order of magnitudes of the different terms in the Hamiltonian are (in a.u.): Coulomb term,  $2 \times 10^{-4}$ ; electric field,  $8 \times 10^{-5}$ ; diamagnetic term,  $2 \times 10^{-4}$ .

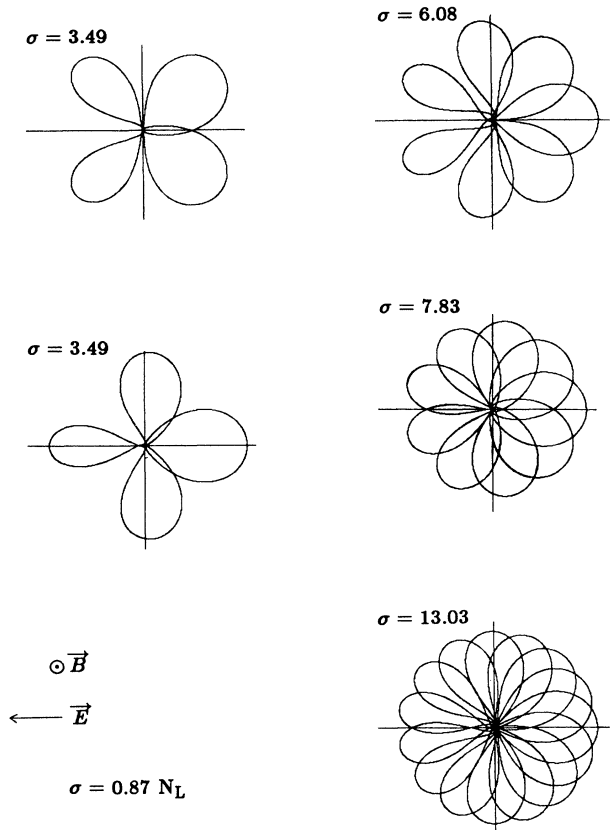


FIG. 13. Periodic trajectories for dominating magnetic field (only a few examples). The scaled electric field  $\epsilon$  is 0.078, and the scaled energy  $\omega$  is 0.490. The scaled actions of the trajectories are indicated.  $N_L$  designates the number of loops the trajectories consist of.

The line strength of the resonances associated with the orbits are rapidly varying functions of the parameters of the scaled spectra. It is not possible to collect resonances to significant groups like in the case of strong electric field. This behavior results from the fact that in the case of strong magnetic field the electron approaches the core nearly after each lobe. Therefore at several locations along the trajectories quantum-mechanical scattering effects show up which cannot be accounted for by semiclassical methods and which strongly depend on energy and field strengths via the impact parameters. Thus the rapid fluctuations of the resonance strength reflect the sensitivity of the scattering cross sections to the parameters of the scan.

## VII. CONCLUSION

In this paper we discussed results on the QL resonances in the spectra of rubidium Rydberg atoms in crossed magnetic and electric fields. The observed resonances are explained completely by semiclassical trajectories. Only those orbits generate resonances that show an overlap with the ground-state wave function and that yield the proper excitation geometry in connection with the laser polarization. The influence of the presented orbits onto the spectra is confirmed by the agreement between dipole moments derived from the trajectories and those following from the Stark structure of the resonances. This is proof also that a good agreement between the semiclassical description and the observed spectra could be obtained.

## ACKNOWLEDGMENTS

The authors thank K. H. Welge and E. Werner for many helpful discussions.

- 
- [1] E. A. Solov'ev, Zh. Eksp. Teor. Fiz. **82**, 1762 (1982) [Sov. Phys. JETP **55**, 1017 (1982)].
- [2] E. A. Solov'ev, Zh. Eksp. Teor. Fiz. **85**, 109 (1983) [Sov. Phys. JETP **58**, 63 (1983)].
- [3] P. A. Braun and E. A. Solov'ev, Zh. Eksp. Teor. Fiz. **86**, 68 (1984) [Sov. Phys. JETP **59**, 38 (1984)].
- [4] P. A. Braun, J. Phys. B **18**, 4187 (1985).
- [5] P. Cacciani, E. Luc-Koenig, J. Pinard, C. Thomas, and S. Liberman, Phys. Rev. Lett. **56**, 1124 (1986).
- [6] P. Cacciani, E. Luc-Koenig, J. Pinard, C. Thomas, and S. Liberman, Phys. Rev. Lett. **56**, 1467 (1986).
- [7] P. Cacciani, S. Liberman, E. Luc-Koenig, J. Pinard, and C. Thomas, J. Phys. B **21**, 3473 (1988).
- [8] P. Cacciani, E. Luc-Koenig, J. Pinard, C. Thomas, and S. Liberman, J. Phys. B **21**, 3499 (1988).
- [9] P. Cacciani, S. Liberman, E. Luc-Koenig, J. Pinard, and C. Thomas, J. Phys. B **21**, 3523 (1988).
- [10] J. Pinard, in *Atoms in Strong Fields*, edited by C. A. Nicolaides, C. W. Clark, and M. H. Nayfeh (Plenum, New York, 1990).
- [11] F. Penent, D. Delande, F. Biraben, and J. C. Gay, Opt. Commun. **49/3**, 184 (1984).
- [12] F. Penent, D. Delande, and J. C. Gay, Phys. Rev. A **37**, 4707 (1988).
- [13] E. Korevaar and M. G. Littman, J. Phys. B **16**, L437 (1983).
- [14] W. R. S. Garton and F. S. Tomkins, Astrophys. J. **158**, 839 (1969).
- [15] A. R. Edmonds, J. Phys. (Paris) Colloq. **31**, C4-71 (1970).
- [16] A. F. Starace, J. Phys. B **6**, 585 (1973).
- [17] J. C. Castro, M. L. Zimmerman, R. G. Hulet, D. Kleppner, and R. R. Freeman, Phys. Rev. Lett. **45**, 1780 (1980).
- [18] J. C. Gay, D. Delande, and F. Biraben, J. Phys. B **13**, L729 (1980).
- [19] N. P. Economou, R. R. Freeman, and P. F. Liao, Phys. Rev. A **18**, 2506 (1978).
- [20] R. R. Freeman and N. P. Economou, Phys. Rev. A **20**, 2356 (1979).
- [21] H. A. Bethe and E. E. Salpeter, *Quantum Mechanics of One- and Two-Electron Atoms* (Springer-Verlag, Berlin, 1957).

- [22] M. Berry, in *Chaotic Behavior of Deterministic Systems*, Les Houches Session 36, edited by G. Iooss, R. H. G. Helleman, and R. Stora (North-Holland, Amsterdam, 1983).
- [23] A. Holle, G. Wiebusch, J. Main, B. Hager, H. Rottke, and K. H. Welge, *Phys. Rev. Lett.* **56**, 2594 (1986).
- [24] J. Main, G. Wiebusch, A. Holle, and K. H. Welge, *Phys. Rev. Lett.* **57**, 2789 (1986).
- [25] G. Wiebusch, J. Main, K. Krüger, H. Rottke, A. Holle, and K. H. Welge, *Phys. Rev. Lett.* **62**, 2821 (1989).
- [26] M. C. Gutzwiller, *J. Math. Phys.* **28/10**, 1979, 1967).
- [27] M. C. Gutzwiller, *J. Math. Phys.* **10/6**, 1004 (1969).
- [28] M. C. Gutzwiller, *J. Math. Phys.* **11/6**, 1791 (1970).
- [29] M. C. Gutzwiller, *J. Math. Phys.* **12/3**, 343 (1971).
- [30] M. C. Gutzwiller, *Physica D* **5**, 183 (1982).
- [31] W. P. Reinhardt, *J. Phys. B* **16**, L635 (1983).
- [32] D. Wintgen, *Phys. Rev. Lett.* **58**, 1589 (1987).
- [33] D. Wintgen and H. Friedrich, *Phys. Rev. A* **36**, 131 (1987).
- [34] D. Wintgen, *Phys. Rev. Lett.* **61**, 1803 (1988).
- [35] D. Wintgen and A. Hoening, *Phys. Rev. Lett.* **63**, 1467 (1989).
- [36] W. Schweizer, R. Niemeier, H. Friedrich, G. Wunner, and H. Rudner, *Phys. Rev. A* **38**, 1724 (1988).
- [37] E. J. Heller, *Phys. Rev. Lett.* **53**, 1515 (1984).
- [38] E. B. Bogomolny, *Physica D* **31**, 169 (1988).
- [39] M. L. Du, J. B. Delos, *Phys. Rev. A* **38**, 1896 (1988).
- [40] M. L. Du, J. B. Delos, *Phys. Rev. A* **38**, 1913 (1988).
- [41] C. W. Clark, E. Korevaar, and M. G. Littman, *Phys. Rev. Lett.* **54**, 320 (1985).
- [42] P. F. O'Mahony, *Phys. Rev. Lett.* **63**, 2653 (1989).